3D Euler Spirals for 3D Curve Completion

Gur Harary
Dept. of Electrical Engineering
Technion
gur@tx.technion.ac.il

Ayellet Tal
Dept. of Electrical Engineering
Technion
ayellet@ee.technion.ac.il

ABSTRACT

Shape completion is an intriguing problem in geometry processing with applications in CAD and graphics. This paper defines a new type of 3D curves, which can be utilized for curve completion. It can be considered as the extension to three dimensions of the 2D Euler spiral. We prove several properties of these curves – properties that have been shown to be important for the appeal of curves. We illustrate their utility in two applications. The first is "fixing" curves detected by algorithms for edge detection on surfaces. The second is shape illustration in archaeology, where the user would like to draw curves that are missing due to the incompleteness of the input model.

Categories and Subject Descriptors

I.3 [**Computer Graphics**]: Computational Geometry and Object Modeling—*Curve, surface, solid, and object representations*

General Terms

Algorithms, Design

Keywords

Euler spirals, 3D curves

1. INTRODUCTION

Shape completion has been an important task in computational geometry with applications to CAD and computer graphics [2, 3, 28]. While most of the work has focused on completing or repairing polyhedra and CAD models, this paper focuses on completing curves in three dimensions. It presents a practical solution to the problem, which is demonstrated by real-life data.

Given two point-tangent pairs, one way to complete them is to use any of the variety of known splines [7, 10]. Such curves possess many attractive properties, however, Figure 1(b) illustrates that they (in this case Hermite splines) might not always produce the preferable results. This is also supported by psychological studies that indicate that splines may be unsatisfactory for curve completion [30].

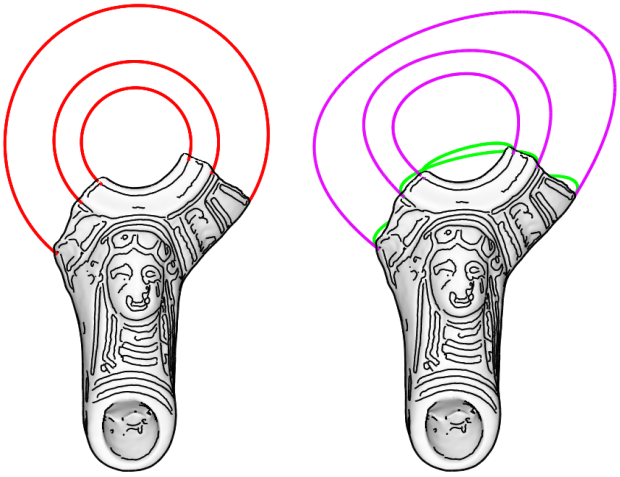

(a) Our completion (b) Hermite completion

Figure 1: 3D Euler spirals (red) complete the curves on a broken Hellenistic oil lamp – curves that would most likely be drawn if the model were complete. The scale of the Hermite splines is determined manually (magenta), since the automatically-scaled splines (green) are inferior due to the large ratio between the length of the curve and the size of the model. Note the perfect circular arcs of our curves.

This paper defines a new type of 3D curves that can be used for this purpose (Figure 1(a)). We show that our curves are not only appealing, but also qualitatively outperform some splines. In a nutshell, our curves can be considered as an extension to 3D of the planar Euler spirals. An important consideration in aesthetic curve design is the curve's fairness [25], which has been shown to be closely related to how little and how smoothly a curve bends. An Euler spiral, also referred to as a *clothoid* or a *Cornu spiral*, is an example of such an aesthetic curve. Its curvature varies linearly with arc-length [16, 20, 21]. Our proposed curve has both its curvature and torsion change linearly with length.

The contribution of this paper is threefold. First, the paper defines the 3D Euler spiral (Section 4) and proves that it satisfies some desirable properties – properties that have been claimed to produce eye-pleasing curves [17] (Section 5).

Permission to make digital or hard copies of all or part of this work for personal or classroom use is granted without fee provided that copies are not made or distributed for profit or commercial advantage and that copies bear this notice and the full citation on the first page. To copy otherwise, to republish, to post on servers or to redistribute to lists, requires prior specific permission and/or a fee.
SCG'10, June 13–16, 2010, Snowbird, Utah, USA.
Copyright 2010 ACM 978-1-4503-0016-2/10/06 ...$10.00.

Figure 2: Archaeological drawing of a broken lamp found in the archaeological site of Dor. This is a manual drawing from [31].

In particular, we prove that our curves are invariant to similarity transformations and that they are symmetric, extensible (i.e., refinable), smooth, and round (i.e., if the boundary conditions lie on a circle, then the curve is a circle, as illustrated in Figure 1(a)). Second, we present a parameter-less algorithm for computing these curves (Section 6). Last but not least, we demonstrate the use of these curves in two curve completion applications (Section 7).

In the first application, our spirals complete curves missing due to "weak" surfaces patches. The second application is curve completion of broken shapes, such as archaeological artifacts. Currently, this task is performed by drawing the missing curves manually in 2D (Figure 2). This is an expensive and time-consuming process, which is prone to biases. Our curves can replace this manual task while performing it in 3D, directly on the scanned artifact. With the growing popularity of digital documentation in archaeology, the ability to draw curves in 3D is becoming ever more important.

2. RELATED WORK

Curve completion: Given two point-tangent pairs, the most common way to perform completion is to use splines, such as a cubic Hermite spline [7, 10]. Splines are fast and easy to compute, but they are not always the curves preferred by the human visual system.

Ullman [32] suggests properties that 2D curves should satisfy: invariance to rigid transformations, smoothness, minimization of the total curvature, and extensibility. These properties led to a Biarc solution – a curve consisting of two circular arcs. Biarcs are smooth and invariant to rigid transformations, but they do not guarantee that the total curvature is minimized and they are not extensible [5]. Biarcs are generalized to 3D in [6, 29].

Knuth [17] proposes different properties of eye-pleasing 2D curves: invariance to similarity transformations and cyclic permutations (for closed curves), extensibility, smoothness, roundness, and being locally constructed. Knuth also shows that the latter four properties cannot take place together. These properties are the base of the METAFONT system of LATEX. [5, 17, 27] propose to use 2D cubic splines, giving up extensibility and roundness.

Another way to construct curves is Elastica [14, 19, 24, 26], which refers to the curves that minimize the total square curvature of the curve: $\mathrm{E}[\kappa(\mathrm{s})] = \int_0^L \kappa^2(s)ds$, where $s \in [0, L]$ is the arc-length parameter and $\kappa(s)$ is the curvature. Horn [14] argues that Elastica is the "smoothest" 2D curve to complete the gap between two point-tangent pairs. It is extensible, but neither scale-variant nor round. Already in 1906 [4] discussed Elastica for 3D curves. A Curve that approximates the solution to Elastica in 3D is explicitly defined in [24]. In 2D this curve is the 2D Euler spiral (discussed next), which has a linear curvature. In 3D, the curvature of this curve is expressed as a hyperbola.

2D Euler spirals: Euler spirals are curves whose curvature evolves linearly along the curve. They were discovered independently by three researchers [20]. In 1694 Bernoulli wrote the equations for the Euler spiral for the first time, but did not draw the spirals or compute them numerically. In 1744 Euler rediscovered the curve's equations, described their properties, and derived a series expansion to the curve's integrals. Later, in 1781, he also computed the spiral's end points. The curves were re-discovered in 1890 for the third time by Talbot, who used them to design railway tracks. Euler spirals are also known as "Cornu spirals" (after Cornu who plotted them) and "Clothoid" (after Clotho, the youngest of the three Fates of Greek mythology). They are defined as the curves that penalize the curvature variation, hence minimizing the following (κ_s is the derivative of κ):

$$\mathrm{E}[\kappa(\mathrm{s})] = \int_0^L \kappa_s^2(s)ds.$$

In [30] psychological experiments show that in 2D an interpolation between two point-tangent pairs using Euler spiral outperforms parabolic curves and circular arcs. This is attributed to its monotonous change in curvature, which has a good fit to the way the human eye interpolates curves.

2D Euler spirals were used in computer aided design. In [14, 23] they are used as an approximation to the solution of Elastica. In [22] the conditions under which the spirals can form a transition curve are investigated. Two spirals are used in [33] to form a parabola-like segment between consecutive points of a control polygon. In [21] a formulation for fitting spiral primitives to a dense polyline data is developed.

In [16] an algorithm is described for 2D curve completion using an Euler spiral. The algorithm is an iterative gradient-descent, initialized by a 2D Biarc. Since there are infinite possible Biarcs, the Biarc that minimizes the total curvature variation is chosen. Some properties that characterize eye-pleasing curves are also proved. In [34] a faster and more accurate algorithm is proposed. It is proved that given two point-tangent pairs, there always exists an Euler spiral that interpolates them.

3D Euler spirals: An attempt to generalize Euler spirals to 3D, maintaining the linearity of the curvature, is presented in [13]. A given polygon is refined, such that the polygon satisfies both arc-length parameterization and linear distribution of the *discrete curvature binormal* vector. The algorithm ignores the torsion, despite being an important characteristic of 3D curves.

We propose a novel algorithm, which produces continu-

ous, rather than discrete, curves and takes both curvature and torsion into account. The algorithm, which is inspired by [16], is general and does not require an initial polygon. We prove that our curve satisfies properties that characterize fair and appealing curves and reduces to the 2D Euler spiral in the planar case.

3. BACKGROUND

A spatial curve $\mathcal{C}(s)$ is determined by its curvature $\kappa(s)$ and its torsion $\tau(s)$. Intuitively, a curve can be obtained from a straight line by bending (curvature) and twisting (torsion).

This section reviews the Frenet-Serret Equations and the Euler-Lagrange Equations, which will be necessary in the derivation of our 3D Euler spirals. In the following, $\vec{T}(s) = \frac{d\mathcal{C}}{ds}(s)$ is the unit tangent vector, $\vec{N}(s)$ is the unit normal vector, and $\vec{B}(s) = \vec{T}(s) \times \vec{N}(s)$ is the binormal vector. We assume an arc-length parameterization.

Frenet-Serret Equations: Given a curvature $\kappa(s) > 0$ and a torsion $\tau(s)$, according to the fundamental theorem of the local theory of curves [9], there exists a unique (up to rigid motion) spatial curve, parameterized by the arc-length s, defined by its Frenet-Serret equations, as follows:

$$\begin{aligned} \frac{d\vec{T}(s)}{ds} &= \kappa(s)\vec{N}(s), \\ \frac{d\vec{N}(s)}{ds} &= -\kappa(s)\vec{T}(s) + \tau(s)\vec{B}(s), \\ \frac{d\vec{B}(s)}{ds} &= -\tau(s)\vec{N}(s). \end{aligned} \tag{1}$$

The curve $\mathcal{C}$ is defined by:

$$\begin{aligned} \mathcal{C}(s) &= \int_0^s \vec{T}(v)\, dv + \mathbf{x}_0 \\ &= \int_0^s \left[\int_0^t \frac{d\vec{T}(u)}{du}\, du + \vec{T}_0 \right] dt + \mathbf{x}_0. \end{aligned} \tag{2}$$

Euler-Lagrange Equation: The Euler-Lagrange Equation is fundamental in *calculus of variations* [11]. It is a differential equation, useful for solving optimization problems in which, given some functional, one seeks the function that optimizes it. It is satisfied by a function q of a real argument s, which is a stationary point of the functional

$$\mathcal{S}(q) = \int_{s_1}^{s_2} \mathcal{L}(s, q(s), q'(s)) ds, \tag{3}$$

where $q = (q_1, \ldots, q_n)$ is the function to be found, $q' = (q_1', \ldots, q_n')$, $q_i' = \frac{dq_i}{ds}$, $i = (1, \ldots, n)$, and the positions $q(s_1)$ and $q(s_2)$ are defined.

The function q that optimizes Equation (3) satisfies the Euler-Lagrange Equations:

$$\frac{d}{dt}\left(\frac{\partial \mathcal{L}}{\partial q_i'}\right) - \frac{\partial \mathcal{L}}{\partial q_i} = 0 \quad (i = 1, \ldots, n). \tag{4}$$

4. 3D EULER SPIRALS

This section defines the 3D Euler spiral – the curve having both its curvature and torsion evolve linearly along the curve (Figure 3). Furthermore, we require that our curve conforms with the definition of a 2D Euler spiral. We start with some intuition, then define the 3D Euler spiral, and finally prove its existence and uniqueness up to a rigid transformation.

Figure 3: A 3D Euler spiral

We seek a functional that will penalize the change in curvature and torsion along the curve. Thus, the curve should minimize the sum of the square variation of the curvature and the torsion. Formally, we require that the following integral be minimized:

$$\mathcal{S}((\kappa, \tau)) = \int_0^L \left[\kappa_s^2(s) + \tau_s^2(s)\right] ds, \tag{5}$$

where L is the curve's length, $\kappa_s = \frac{\partial \kappa}{\partial s}$, and $\tau_s = \frac{\partial \tau}{\partial s}$. Note that in the planar case $\tau = 0$, therefore our definition indeed conforms with the definition of the 2D Euler spiral.

Minimizing Equation (5) can be performed using the Euler-Lagrange Equation. In our case, Equation (5) corresponds to Equation (3) as follows:

$$\begin{aligned} &q_1(s) \mapsto \kappa(s), \\ &q_1'(s) \mapsto \kappa_s(s), \\ &q_2(s) \mapsto \tau(s), \\ &q_2'(s) \mapsto \tau_s(s), \\ &\mathcal{L}\left(s, q(s), q'(s)\right) \mapsto \left[\kappa_s^2(s) + \tau_s^2(s)\right]. \end{aligned}$$

Hence, the corresponding Euler-Lagrange Equations are (by Equation (4)):

$$\kappa: \quad \frac{d}{ds}\left(\frac{\partial(\kappa_s^2 + \tau_s^2)}{\partial \kappa_s}\right) = 0 \;\Rightarrow\; \frac{d}{ds}(2\kappa_s) = 0 \;\Rightarrow\; \kappa_{ss} = 0,$$

$$\tau: \quad \frac{d}{ds}\left(\frac{\partial(\kappa_s^2 + \tau_s^2)}{\partial \tau_s}\right) = 0 \;\Rightarrow\; \frac{d}{ds}(2\tau_s) = 0 \;\Rightarrow\; \tau_{ss} = 0.$$

By integrating κ_{ss} and τ_{ss} twice, these equations lead to a curve whose curvature and torsion evolve linearly. Thus, for some constants $\kappa_0, \tau_0, \gamma, \delta \in \mathbb{R}$, and for $0 \le s \le L$:

$$\kappa(s) = \kappa_0 + \gamma s, \quad \tau(s) = \tau_0 + \delta s. \tag{6}$$

In summary, we have shown that the curve that minimizes our functional (Equation (5)) is a curve whose curvature and torsion change linearly along the curve. Note that since our curve has a linear relation between the curvature and torsion, it is a special case of Bertrand curves [12]. This, however, neither helps in deriving the properties proved in Section 5 (which do not hold for general Bertrand curves) nor provides a method for constructing them (Section 6).

Next, we define the curve that satisfies Equation (6). This definition is in the form of a set of differential equations. We assume that we are given the following initial conditions: a point $\mathbf{x}_0$ on the curve, a tangent $\vec{T}_0$ at $\mathbf{x}_0$, and a normal $\vec{N}_0$.

DEFINITION 4.1. **3D Euler spiral:** *The 3D curve that satisfies Equation* (6) *and the initial conditions is the curve* $\mathcal{C}$*, for which the following conditions hold:*

1. $\frac{d\mathcal{C}(s)}{ds} = \vec{T}(s)$,
2. $\frac{d\vec{T}(s)}{ds} = (\kappa_0 + \gamma s)\vec{N}(s)$,
3. $\frac{d\vec{N}(s)}{ds} = -(\kappa_0 + \gamma s)\vec{T}(s) + (\tau_0 + \delta s)\vec{B}(s)$,
4. $\frac{d\vec{B}(s)}{ds} = -(\tau_0 + \delta s)\vec{N}(s)$,
5. $\mathcal{C}(0) = \mathbf{x}_0$, $\vec{T}(0) = \vec{T}_0$, $\vec{N}(0) = \vec{N}_0$, $\vec{B}(0) = \vec{T}_0 \times \vec{N}_0$.

To understand this definition, observe that 1 is the definition of the tangent, 2–4 are the Frenet-Serret Equations with our curvature and torsion, and 5 represents the initial conditions.

Finally, the following proposition proves the existence of this curve and its uniqueness up to a rigid transformation.

PROPOSITION 4.1. *Given constants* $\kappa_0, \tau_0, \gamma, \delta, \in \mathbb{R}$*, there exists a 3D Euler spiral having a linear curvature* $\kappa(s) = \kappa_0 + \gamma s$ *and a linear torsion* $\tau(s) = \tau_0 + \delta s$*. Moreover, this curve is unique up to a rigid transformation.*

PROOF. By definition of the curvature of curves in $\mathbb{R}^3$, $\kappa(s) = \left|\frac{d^2\vec{C}}{ds^2}(s)\right| \geq 0$. According to the fundamental theorem of local theory of curves, for every differential function with $\kappa(s) > 0$ and $\tau(s)$, there exists a regular parameterized curve, where $\kappa(s)$ is the curvature, $\tau(s)$ is the torsion, and s is the arc-length parameterization [9]. Moreover, any other curve satisfying the same conditions, differs by a rigid motion.

If $\kappa(s) = 0\ \forall s$, the curve is a straight line, which is unique up to a rigid transformation. It is also possible that $\kappa(s) = 0$ for a single point. In this case, the tangent and hence the curve are well-defined at this point, which is the inflection point at which the normal switches directions. (Note that by our definition $\kappa(s)$ may be negative. In this case, we consider $|\kappa(s)|$ and regard the switch of the sign as a change of the normal direction.) □

5. PROPERTIES OF 3D EULER SPIRALS

The aesthetics of curves has been studied in a variety of papers [16, 17, 32]. In addition to having its curvature and torsion change linearly – a property acknowledged to characterize eye-pleasing curves – this section proves that our 3D Euler curves also hold the following properties.

1. Invariance to similarity transformations (translation, rotation, and scaling).
2. Symmetry: The curve leaving the point $\mathbf{x}_0$ with tangent $\vec{T}_0$ and reaching the point $\mathbf{x}_f$ with tangent $\vec{T}_f$, coincides with the curve leaving the point $\mathbf{x}_f$ with tangent $-\vec{T}_f$ and reaching the point $\mathbf{x}_0$ with tangent $-\vec{T}_0$.
3. Extensibility: For every point $\mathbf{x}_m \in \mathcal{C}$ between points $\mathbf{x}_0$ and $\mathbf{x}_f$, the curves $\mathcal{C}_1$ between $\mathbf{x}_0$ and $\mathbf{x}_m$ and $\mathcal{C}_2$ between $\mathbf{x}_m$ and $\mathbf{x}_f$ coincide with $\mathcal{C}$, each in its own section.
4. Smoothness: The tangent is defined at every point, i.e., $\frac{\partial\mathcal{C}}{\partial s}$ is finite. (In fact, our curves are C^∞-smooth.)
5. Roundness: If $\mathcal{C}$ interpolates two point-tangent pairs lying on a circle, then $\mathcal{C}$ is a circle. The importance of this property is demonstrated in Figures 1,6–7, where our spirals are both appealing and correct, since the boundary conditions indicate completion by a circular arc.

PROPOSITION 5.1. *A 3D Euler spiral is invariant to similarity transformations.*

PROOF. Invariance to rotation and translation results from Proposition 4.1. Below we prove invariance to scale. We are given an Euler spiral $\mathcal{C}$ of length L, which interpolates $\mathbf{x}_0 = \mathcal{C}(0)$ and $\mathbf{x}_f = \mathcal{C}(L)$, and whose parameters are $\kappa_0, \tau_0, \gamma, \delta$. We should show that the spiral $\mathcal{C}_\lambda$, which interpolates $\lambda\mathbf{x}_0$ and $\lambda\mathbf{x}_f$ for $\lambda > 0$, is equal to $\mathcal{C}$ multiplied by λ, i.e., $\forall s, 0 \leq s \leq L$:

$$\mathcal{C}_\lambda(s) = \lambda\mathcal{C}(s). \tag{7}$$

Hence, we need to find the constants $\widetilde{\kappa_0}, \widetilde{\tau_0}, \widetilde{\gamma}, \widetilde{\delta}, \widetilde{L}$ that define an Euler spiral $\mathcal{C}_\lambda$ that passes through $\lambda\mathbf{x}_0$ and $\lambda\mathbf{x}_f$ (i.e., $\mathcal{C}_\lambda(0) = \lambda\mathbf{x}_0$ and $\mathcal{C}_\lambda(\lambda L) = \lambda\mathbf{x}_f$) with tangents $\vec{T}_0$ and $\vec{T}_f$ respectively. Moreover, for every point on the curve, it should coincide with $\lambda\mathcal{C}$.

We examine the 3D Euler spiral that satisfies Definition 4.1, having parameters $\widetilde{\kappa_0} = \frac{\kappa_0}{\lambda}, \widetilde{\tau_0} = \frac{\tau_0}{\lambda}, \widetilde{\gamma} = \frac{\gamma}{\lambda^2}$, $\widetilde{\delta} = \frac{\delta}{\lambda^2}, \widetilde{L} = \lambda L$. According to 2–4 in Definition 4.1, we get:

$$\begin{aligned}
\frac{d\vec{T}(u)}{du} &= \left(\frac{\kappa_0}{\lambda} + \frac{\gamma}{\lambda^2}u\right)\vec{N}(u), \\
\frac{d\vec{N}(u)}{du} &= -\left(\frac{\kappa_0}{\lambda} + \frac{\gamma}{\lambda^2}u\right)\vec{T}(u) + \left(\frac{\tau_0}{\lambda} + \frac{\delta}{\lambda}u\right)\vec{B}(u), \\
\frac{d\vec{B}(u)}{du} &= -\left(\frac{\tau_0}{\lambda} + \frac{\delta}{\lambda^2}u\right)\vec{N}(u).
\end{aligned} \tag{8}$$

By defining a new parameter $v = u/\lambda$ ($\Rightarrow dv = du/\lambda$), we get that $\frac{d\vec{T}}{du} = \frac{d\vec{T}}{dv}\frac{dv}{du} = \frac{1}{\lambda}\frac{d\vec{T}}{dv}$. Similarly, $\frac{d\vec{N}}{du} = \frac{1}{\lambda}\frac{d\vec{N}}{dv}$ and $\frac{d\vec{B}}{du} = \frac{1}{\lambda}\frac{d\vec{B}}{dv}$. Equation (8) now becomes:

$$\begin{aligned}
\frac{d\vec{T}(v)}{dv} &= (\kappa_0 + \gamma v)\vec{N}(v), \\
\frac{d\vec{N}(v)}{dv} &= -(\kappa_0 + \gamma v)\vec{T}(v) + (\tau_0 + \delta v)\vec{B}(v), \\
\frac{d\vec{B}(v)}{dv} &= -(\tau_0 + \delta v)\vec{N}(v).
\end{aligned}$$

Note that this could be done since all the properties of the Frenet-Serret Equations hold for every parameterization, not necessarily the arc-length parameterization [9] .

We can now proceed to calculating the 3D Euler spiral and its tangent:

$$\vec{T}_\lambda(s) = \int_0^{\lambda s} \frac{d\vec{T}}{du}du + \vec{T}_0,$$

$$\mathcal{C}_\lambda(s) = \int_0^{\lambda s}\left[\int_0^t \frac{d\vec{T}}{du}du + \vec{T}_0\right]dt + \lambda\mathbf{x}_0.$$

By defining new parameters $v = u/\lambda (\Rightarrow dv = du/\lambda)$ and $\hat{t} = t/\lambda (\Rightarrow d\hat{t} = dt/\lambda)$, we get:

$$\vec{T}_\lambda(s) \overset{v=u/\lambda}{=} \int_0^s \frac{1}{\lambda}\frac{d\vec{T}}{dv}\lambda dv + \vec{T}_0 = \vec{T}(s),$$

$$\begin{aligned}\mathcal{C}_\lambda(s) &\overset{v=u/\lambda}{=} \int_0^{\lambda s}\left[\int_0^{t/\lambda}\frac{1}{\lambda}\frac{d\vec{T}}{dv}\lambda dv + \vec{T}_0\right]dt + \lambda\mathbf{x}_0 \\ &\overset{\hat{t}=t/\lambda}{=} \int_0^{s}\left[\int_0^{\hat{t}}\frac{d\vec{T}}{dv}dv + \vec{T}_0\right]\lambda d\hat{t} + \lambda\mathbf{x}_0 \\ &= \lambda\mathcal{C}(s).\end{aligned}$$

Since this holds for every $0{\leq}s{\leq}L$, Equation (7) holds. We also specifically get the boundary conditions $\mathcal{C}_\lambda(0) = \lambda\mathcal{C}(0) = \lambda\mathbf{x}_0, \vec{T}_\lambda(0) = \vec{T}(0) = \vec{T}_0$ and $\mathcal{C}_\lambda(\lambda L) = \lambda\mathcal{C}(L) = \lambda\mathbf{x}_f, \vec{T}_\lambda(\lambda L) = \vec{T}(L) = \vec{T}_f$. □

PROPOSITION 5.2. *A 3D Euler spiral is symmetric. (Proof in Appendix A)*

PROPOSITION 5.3. *A 3D Euler spiral is extensible. (Proof in Appendix B)*

PROPOSITION 5.4. *A 3D Euler spiral is smooth.*

PROOF. According to Proposition 4.1, there exists a solution for the Frenet-Serret equations. Therefore, $\frac{\partial\mathcal{C}}{\partial s} = \vec{T}(s)$ is defined for every $0{\leq}s{\leq}L$. □

PROPOSITION 5.5. *A 3D Euler spiral is round.*

PROOF. For given two point-tangent pairs lying on a circle, the circle defined by $\kappa_0 \neq 0, \tau_0 = 0, \gamma = 0, \delta = 0$ is a solution for the Frenet-Serret Equation. □

6. CURVE CONSTRUCTION ALGORITHM

In Section 4 we have shown that given curve parameters $\kappa_0, \tau_0, \gamma, \delta, L \in \mathbb{R}$ and initial conditions $\mathbf{x}_0$, $\vec{T}_0$ and $\vec{N}_0$, there exists a 3D Euler spiral determined by these parameters and satisfying the initial conditions.

In practice, however, we are given two points and their associated tangents $\left(\mathbf{x}_0, \vec{T}_0\right)$ and $\left(\mathbf{x}_f, \vec{T}_f\right)$. Our goal is to find the parameters $\kappa_0, \tau_0, \gamma, \delta, L \in \mathbb{R}$ that define the 3D Euler spiral that starts at $\mathbf{x}_0$ and $\vec{T}_0$ and minimizes both the difference between the curve's position at $s = L$ and $\mathbf{x}_f$, and the difference between the curve's tangent at $s = L$ and $\vec{T}_f$. In other words, we attempt to minimize the following error:

$$\epsilon = (\epsilon_x + \epsilon_T), \tag{9}$$

$$\epsilon_x = \left[(x(L) - x_f)^2 + (y(L) - y_f)^2 + (z(L) - z_f)^2\right],$$

$$\epsilon_T = \left[(T_x(L) - T_{f,x})^2 + (T_y(L) - T_{f,y})^2 + (T_z(L) - T_{f,z})^2\right].$$

We experimented with other weights of ϵ_x and ϵ_T as well, but they were not proven beneficial.

We propose the Gradient-descent approach to find the parameters of the 3D Euler spiral that minimizes the error in Eq. (9). This approach, which guarantees convergence to a local minimum, is described below and explained thereafter.

Parameter initialization (Step 1): The 3D Euler spiral is initialized using a planar Euler spiral [34]. The question is which plane to choose. We define the plane for which three out of the four boundary conditions hold: $\mathbf{x}_0$, $\mathbf{x}_f$, and $\vec{T}_0$. Therefore, the plane (whose normal is denoted by $\vec{N}_0$) is defined by two vectors: $\vec{T}_0$ and the vector between $\mathbf{x}_0$ and $\mathbf{x}_f$. Note that the resulting planar Euler spiral interpolates

Algorithm 1 Gradient-descent 3D Euler spiral construction

1: Parameter initialization $< \kappa_0, \tau_0, \gamma, \delta, L >$
2: While the current error ϵ and the current step size Δ are large:
3: Calculate the gradient direction
4: Define the step size Δ
5: Update the curve parameters $< \kappa_0, \tau_0, \gamma, \delta, L >$

$\vec{T}_0$ at $\mathbf{x}_0$ and the projection of $\vec{T}_f$ onto the plane at $\mathbf{x}_f$. The parameters of this 2D spiral κ_0, γ, L are used to initialize our curves. Since it lies on a plane, the torsion's parameters are initialized to zero ($\tau_0 = 0$, $\delta = 0$).

Our experiments indicate that this initialization gives a good approximation to κ_0 and γ, which hardly change afterwards. We also tested other initialization methods (e.g., Hermite spline, 3D Biarc, and 2D Euler spiral on the binormal plane). We found that our initialization is the fastest and the most accurate.

Iterative step (Steps 3-5): First, the gradient direction, which is the direction of the steepest descent, is calculated. Since the curve is described as a set of differential equations that do not have an explicit solution, we cannot explicitly find the best gradient direction. Instead, at each iteration, we first find the parameters among $\kappa_0, \tau_0, \gamma, \delta, L$, that when modified by $\pm\Delta$, yield a decrease of the error ϵ. We then compare the Euler spirals that result by modifying only one of these parameters to the spiral that results by modifying them all, and choose the spiral that obtains the minimum error ϵ.

Each of these candidate curves is computed by numerically solving the Frenet-Serret Equations (Definition 4.1). This is done by sampling the arc-length parameter s uniformly and solving the equations at these sampled points, using the Euler method [1]. This method only needs the solution at the immediately preceding point to compute the function at the next point. The first point is the input $\mathbf{x}_0$, $\vec{T}_0$ and the normal to the initial plane $\vec{N}_0$ (from Step 1).

Next, the step size is modified. If the error ϵ of the chosen direction is smaller than the error obtained in the previous iteration, Δ is unchanged. Otherwise, it is decreased to $\frac{3\Delta}{4}$.

Finally, the parameters are updated. If Δ is unchanged, the parameters that determined the gradient direction are updated according to the chosen direction.

Termination (Step 2): In our experiments, Δ is initialized to 0.1. The algorithm runs until Δ *<1e-5* or the error ϵ *<1e-6*. Smaller values yield negligible changes to the curves.

Optional bound on L (Step 5): Since our curve is a spiral, the obtained solution can have multiple revolutions. For the type of input we expect, it is often desirable to limit the solution to have at most one revolution. This is done by bounding the parameter L, as follows. We first approximate the maximal possible length as the length of the planar Euler spiral with parameters κ_0, γ. Since the tangent angle of such a curve is $\theta(s) = \frac{1}{2}\gamma s^2 + \kappa_0 s + \theta_0$ [16], we require that

$$\theta(L) - \theta_0 = \frac{1}{2}\gamma L^2 + \kappa_0 L \leq 2\pi.$$

Implementation issues: Calculating the numerical solution to the Frenet-Serret Equations at each iteration of the Gradient-descent algorithm might be expensive. In addition,

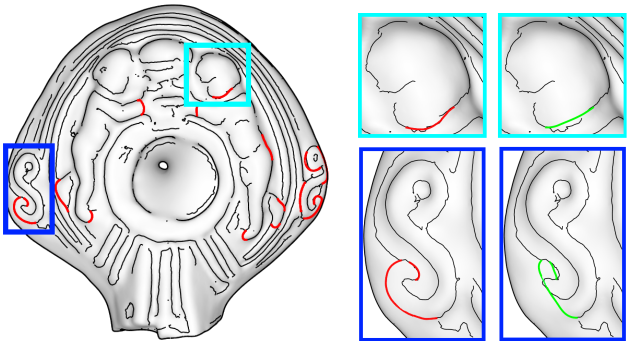

Figure 4: Fixing the curves detected by [18]. Our curves (red) manage to capture the "S" shape, in contrast to the automatically-scaled Hermite splines (green).

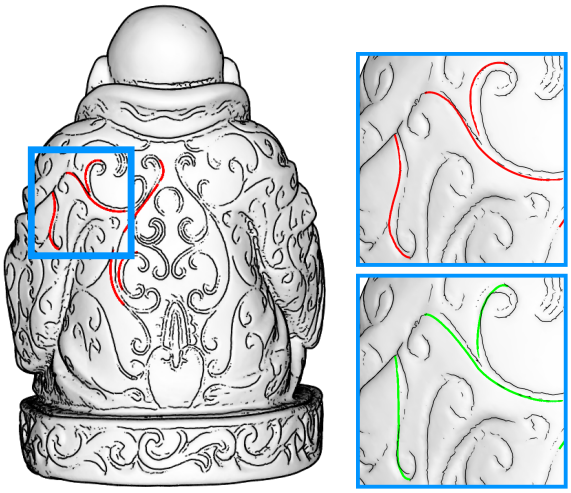

Figure 5: Completing the curves produced by [8] on the Buddha – 3D Euler spirals (red) and Hermite splines (green). Note how the spirals nicely capture the "S" shapes.

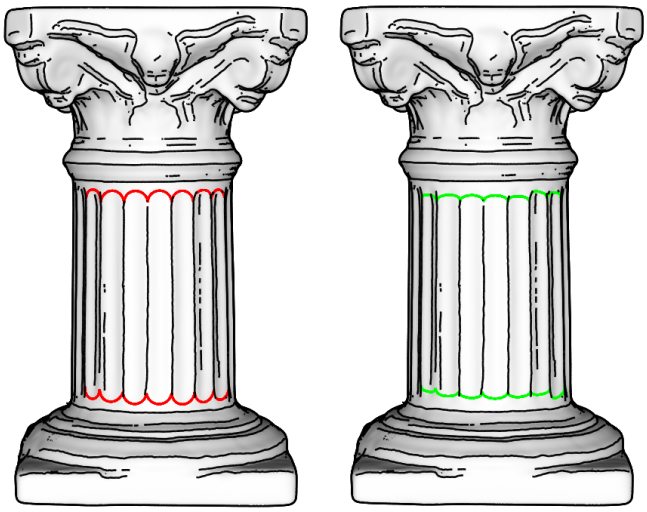

(a) Our completion (b) Hermite completion

Figure 6: Completing the curves produced by [15] on the Column model: Our Euler-spiral completion (red) is circular and resembles the real column.

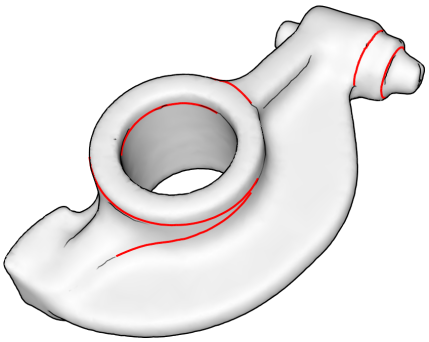

Figure 7: Completing the curves produced by [8] on the Rocker-arm model. The roundness property is visible.

the number of samples along the curve should be carefully determined. Using too many samples will result in a long computation time, while too few samples will cause accuracy problems and result in a large error ϵ. To accelerate the computation while using a fixed and rather small number of samples, we scale the region of interest to the box $(-1,-1,-1)$,$(1,1,1)$, prior to applying Algorithm 1, and then scale it back. Recall that Proposition 5.1 allows us to scale the problem back and forth.

In practice, the problem is first translated by $-x_0$. Then, it is scaled by $D = \max(\triangle x = |x_f - x_0|, \triangle y = |y_f - y_0|, \triangle z = |z_f - z_0|)$, while leaving the tangents at the endpoints unaltered. Then, the curve's parameters are found by Algorithm 1 using 100 samples along the curve for performing the numerical calculations. Once a solution is obtained, it is scaled back to the original range.

7. RESULTS AND APPLICATIONS

This section demonstrates the use of our spirals in two curve completion applications. In the first, the entire model is given, but the algorithm for edge detection on surfaces generates incomplete curves. This is a common problem with most edge-detection algorithms, which may be vital for the shape analysis algorithms that use these curves. In the second application, the given models are broken – a situation prevalent in archaeology. The user is interested in drawing the curves that would be drawn should the entire model be given. In both cases, the user needs only mark the endpoints of the curves and the system creates an Euler spiral between the given endpoints. No parameter tuning is necessary.

Curve completion on polyhedral surfaces: Figures 4–7 demonstrate the use of our spirals for completing the curves detected by various edge detection algorithms: suggestive contours [8], apparent ridges [15], valleys and ridges [35], and demarcating curves [18]. In this application the user needs only choose the endpoints of existing curves that should be connected, since the system can automatically compute the tangents at these endpoints.

Our curves are also compared to the results obtained using Hermite splines. Since Hermite splines depend on the magnitude of the tangent, we used automatic scaling. The

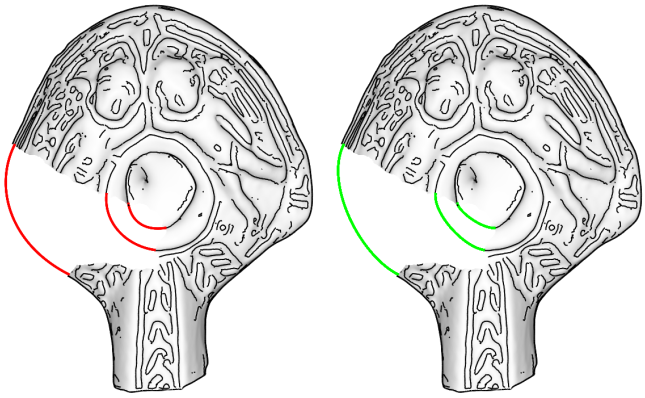

(a) Our completion (b) Hermite completion

Figure 8: Completing a (manually) broken lamp. The 3D Euler spirals (red) are more appealing than the Hermite splines (green) due to the nice circles produced. This is guaranteed by the roundness property of our curves.

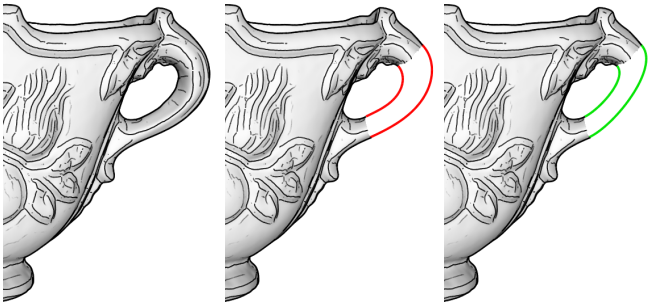

(a) Unbroken model (b) Our completion (c) Hermite

Figure 9: The completion of a (manually) broken pot. Our curves better resemble the original unbroken model.

tangents provided for the computation of the Hermite splines are multiplied by D (described in Section 6), so as to relate their length to the distance between the endpoints.

It can be seen that our curves manage to satisfactorily complete the curves, regardless of how they were created. The two features that are most visible in our spirals, are the ability to create perfect circular arcs (Figures 6– 7) and the "natural" S-shapes (Figure 5).

In this application, the generated curves should lie on the surface. Since our curves are not constrained to lie on any surface, the produced 3D Euler curves are projected to the surface. This is done by projecting each point on the curve to its closest point onto the mesh. Though this method is straightforward, it yields good results.

Shape illustration in archaeology: Archaeology sets many challenges to geometry processing. Many of the artifacts found by the archaeologists are scanned and need to be processed and analyzed. These artifacts are often broken and eroded and thus are difficult to handle. One specific problem is the drawing of the artifact, which is traditionally performed manually by archaeological artists in 2D, as shown in Figure 2. This is an expensive and time-consuming procedure, which is prone to biases and inaccuracies. Our curves propose a 3D alternative, as illustrated in Figure 8.

Figures 9–11 show several additional models, which show that our completed curves are not only more appealing, but also better resemble the shape of the original unbroken models. For example, the curl completion in Figure 10 demonstrates the S-shape property of our spirals, while the ear completion illustrates a more "circular" shape. Figure 11 demonstrates that since our curves have more "volume", they avoid intersecting the mesh, which might occur when using the Hermite completion.

Running times: The algorithm was implemented in Matlab and C and ran on a 2Ghz Intel Core 2 Duo-processor laptop with 2Gb of memory. The running time, which depends on the complexity of the required interpolation curve, is 0.01–0.5 second for the curves demonstrated in this paper. The further the curve is from being planar, the longer the time required. This is probably due to initializing the torsion to zero. The size of the model has little affect on the time; it is relevant only when projection is performed. The projection itself is straightforward and quick to compute.

8. CONCLUSION

This paper presented a novel definition of curves, which extends the 2D Euler spiral to 3D. We proved that for given parameters, a unique curve always exists. Moreover, we showed that our curves satisfy several desired aesthetic properties, including invariance to similarity transformation, symmetry, extensibility, smoothness, and roundness. Given boundary conditions – endpoints and tangents – this paper proposed a novel technique for generating these curves, based on the gradient-descent approach.

The utility of our curves is demonstrated for edge completion on polyhedral surfaces and for artifact illustration in archaeology – a task that is traditionally performed manually in 2D. In archaeology, when automatic 3D curve drawing replaces the traditional manual 2D drawing, automatic or interactive curve completion, would be the only alternative. We believe that the proposed curves may be found a feasible alternative for additional applications involving shape design, artistic design, and shape analysis.

In the future, we wish to prove existence of the curves given point–tangent boundary conditions. In 2D, an algorithm was first established [16] before existence was proved several years later [34]. We hope that the same will happen in 3D. In practice a solution exists for all the inputs we tried.

Acknowledgements: This research was supported in part by the Israel Science Foundation (ISF) 628/08, the Goldbers Fund for Electronics Research, and the Ollendorff foundation. We thank Dr. A. Gilboa and the Zinman Institute of Archaeology at the University of Haifa for providing the archaeological models.

9. REFERENCES

[1] U. Ascher and L. Petzold. *Computer methods for ordinary differential equations and differential-algebraic equations*. Society for Industrial Mathematics, 1998.

[2] G. Barequet and S. Kumar. Repairing CAD models. In *IEEE Visualization*, 1997.

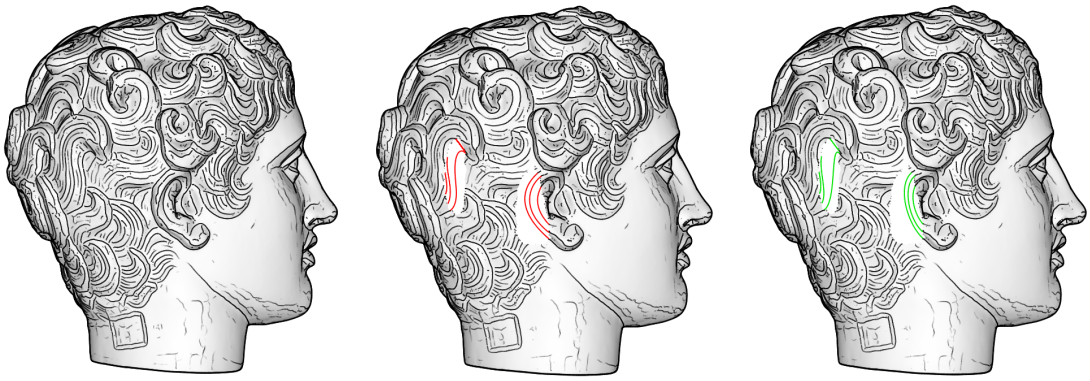

(a) Unbroken model (b) Our completion (c) Hermite completion

Figure 10: Completing a (manually) broken head sculpture. The 3D Euler spirals (red) nicely compute the S-shaped curl. The Euler completion of both the curl and the ear are more similar to the original model than the Hermite completion (green).

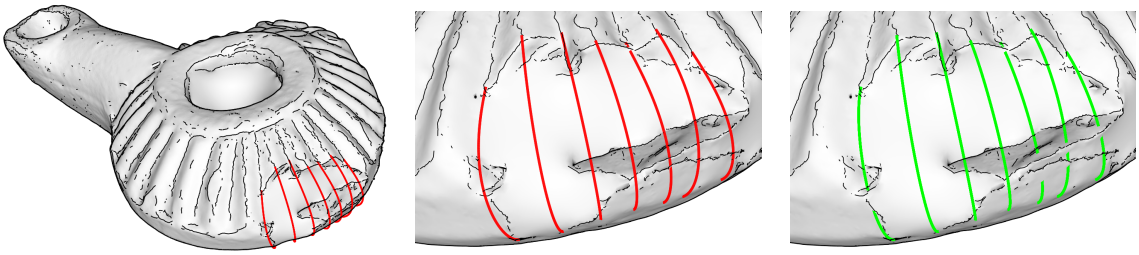

(a) Our completion (b) Zoom in - our completion (c) Hermite completion

Figure 11: Completion of a broken Hellenistic lamp. The curves produced by [35] are used to determine initial conditions. Our curves (red) manage to capture the true volume of the shape, while the Hermite splines (green) intersect the broken model.

[3] G. Barequet and M. Sharir. Filling gaps in the boundary of a polyhedron. *Computer Aided Geometric Design*, 12(2):207–229, 1995.

[4] M. Born. *Untersuchungen über die Stabilität der elastischen Linie in Ebene und Raum: Unter verschiedenen Grenzbedingungen*. Dieterich, 1906.

[5] M. Brady, W. Grimson, and D. Langridge. Shape encoding and subjective contours. In *First Annual National Conference on Artificial Intelligence*, pages 15–17, 1980.

[6] K. Chui, W. Chiu, and K. Yu. Direct 5-axis tool-path generation from point cloud input using 3D biarc fitting. *Robotics and Comp. Integrated Manufacturing*, 24(2):270–286, 2008.

[7] C. De Boor. *A practical guide to splines*. Springer, 2001.

[8] D. DeCarlo, A. Finkelstein, S. Rusinkiewicz, and A. Santella. Suggestive contours for conveying shape. *ACM Trans. Graph.*, 22(3):848–855, 2003.

[9] M. do Carmo. *Differential geometry of curves and surfaces*. Prentice Hall, 1976.

[10] G. Farin. *Curves and surfaces for computer aided geometric design*. Academic Press Professional Inc., 1993.

[11] A. Forsyth. *Calculus of variations*. Dover, NY, 1960.

[12] W. Graustein. *Differential Geometry*. Dover, 2006.

[13] L. Guiqing, L. Xianmin, and L. Hua. 3D discrete clothoid splines. In *CGI '01*, pages 321–324, 2001.

[14] B. Horn. The curve of least energy. *ACM Transactions on Mathematical Software*, 9(4):441–460, 1983.

[15] T. Judd, F. Durand, and E. Adelson. Apparent ridges for line drawing. *ACM Trans. Graph.*, 26(3):19:1–7, 2007.

[16] B. Kimia, I. Frankel, and A. Popescu. Euler spiral for shape completion. *Int. J. Comp. Vision*, 54(1):159–182, 2003.

[17] D. Knuth. Mathematical typography. *American Mathematical Society*, 1(2):337–372, 1979.

[18] M. Kolomenkin, I. Shimshoni, and A. Tal. Demarcating curves for shape illustration. *ACM Trans. Graph.*, 27(5):157:1–9, 2008.

[19] R. Levien. The Elastica: a mathematical history. Technical Report UCB/EECS-2008-103, EECS Department, University of California, Berkeley, 2008.

[20] R. Levien. The Euler spiral: a mathematical history. Technical Report UCB/EECS-2008-111, EECS Department, University of California, Berkeley, 2008.

[21] J. McCrae and K. Singh. Sketching piecewise clothoid curves. In *Sketch-Based Interfaces and Modeling*, 2008.

[22] D. Meek and D. Walton. Clothoid spline transition spirals. *Mathematics of Computation*, 59(199):117–133, 1992.

[23] E. Mehlum. Nonlinear splines. *Computer aided geometric design*, pages 173–207, 1974.

[24] E. Mehlum. Appell and the apple (nonlinear splines in space). In *Mathematical Methods for Curves and Surfaces*, pages 365–384, 1995.

[25] H. Moreton and C. Séquin. Functional optimization for fair surface design. *SIGGRAPH*, 26(2):167–176, 1992.

[26] D. Mumford. Elastica and computer vision. *Algebraic Geometry and Its Applications*, pages 491–506, 1994.

[27] W. Rutkowski. Shape completion. *Computer Graphics and Image Processing*, 9:89–101, 1979.

[28] A. Sharf, M. Alexa, and D. Cohen-Or. Context-based surface completion. *ACM Trans. Graph.*, 23(3):878–887, 2004.

[29] T. Sharrock and R. Martin. Biarc in three dimensions. In *The mathematics of surfaces II*, pages 395–411, 1996.

[30] M. Singh and J. Fulvio. Visual extrapolation of contour geometry. *Natl. Academy of Sciences*, 102(3):939–944, 2005.

[31] E. Stern. *Excavations at Dor*. Jerusalem: Institute of Archaeology of the Hebrew University, 1995.

[32] S. Ullman. Filling-in the gaps: The shape of subjective contours and a model for their generation. *Biological Cybernetics*, 25(1):1–6, 1976.

[33] D. Walton and D. Meek. A controlled clothoid spline. *Computers & Graphics*, 29(3):353–363, 2005.

[34] D. Walton and D. Meek. G1 interpolation with a single cornu spiral segment. *Journal of Computational and Applied Mathematics*, 223(1):86–96, 2007.

[35] S. Yoshizawa, A. Belyaev, and H. P. Seidel. Fast and robust detection of crest lines on meshes. In *ACM Symposium on Solid and Physical Modeling*, pages 227–232, 2005.

APPENDIX

A. SYMMETRY (PROPOSITION 5.3)

Proof: We are given a 3D Euler spiral $\mathcal{C}$ that interpolates the point-tangent pairs $(\mathbf{x}_0, \vec{T}_0)$ and $(\mathbf{x}_f, \vec{T}_f)$ and has parameters $\kappa_0, \tau_0, \gamma, \delta, L$. We need to show that the 3D Euler spiral $\mathcal{C}_{sym}$ that interpolates the point-tangent pairs $(\mathbf{x}_f, -\vec{T}_f)$ and $(\mathbf{x}_0, -\vec{T}_0)$ coincides with $\mathcal{C}$.

Thus, we need to find the constants $\widetilde{\kappa_0}, \widetilde{\tau_0}, \widetilde{\gamma}, \widetilde{\delta}, \widetilde{L}$ that define the Euler spiral $\mathcal{C}_{sym}$ and show that at every point the curves coincide and their tangents are opposite:

$$\vec{T}_{\mathcal{C}_{sym}}(L-s) = -\vec{T}_{\mathcal{C}}(s) \;\; \forall s, 0 \leq s \leq L,$$

$$\mathcal{C}_{sym}(L-s) = \mathcal{C}(s) \;\; \forall s, 0 \leq s \leq L.$$

We examine the 3D Euler spiral $\mathcal{C}_{sym}$ that satisfies Definition 4.1 and has parameters $\widetilde{\kappa_0} = \kappa_0 + \gamma L$, $\widetilde{\tau_0} = \tau_0 + \delta s$, $\widetilde{\gamma} = -\gamma$, $\widetilde{\delta} = -\delta$, $\widetilde{L} = L$.

According to 2–4 in Definition 4.1, we get:

$$\begin{aligned}
\frac{d\vec{T}_{\mathcal{C}_{sym}}(u)}{du} &= (\kappa_0 + \gamma L - \gamma u)\, \vec{N}_{\mathcal{C}_{sym}}(u), \\
\frac{d\vec{N}_{\mathcal{C}_{sym}}(u)}{du} &= -(\kappa_0 + \gamma L - \gamma u)\, \vec{T}_{\mathcal{C}_{sym}}(u) \\
&\quad + (\tau_0 + \delta L - \delta u)\, \vec{B}_{\mathcal{C}_{sym}}(u), \\
\frac{d\vec{B}_{\mathcal{C}_{sym}}(u)}{du} &= -(\tau_0 + \delta L - \delta u)\, \vec{N}_{\mathcal{C}_{sym}}(u).
\end{aligned} \tag{10}$$

By defining a new parameter $v = L - u$ ($\Rightarrow dv = -du$), we get that $\frac{d\vec{T}_{\mathcal{C}_{sym}}}{du} = \frac{d\vec{T}_{\mathcal{C}_{sym}}}{dv}\frac{dv}{du} = -\frac{d\vec{T}_{\mathcal{C}_{sym}}}{dv} = \frac{d\vec{T}_{\mathcal{C}}}{dv}$. Similarly, $\frac{d\vec{N}_{\mathcal{C}_{sym}}}{du} = -\frac{d\vec{N}_{\mathcal{C}_{sym}}}{dv}$ and $\frac{d\vec{B}_{\mathcal{C}_{sym}}}{du} = -\frac{d\vec{B}_{\mathcal{C}_{sym}}}{dv}$. This could be done since all the properties of the Frenet-Serret Equations hold for every parameterization, not necessarily the arc-length parameterization [9] . By tangent definition we get:

$$\begin{aligned}
&\vec{T}_{\mathcal{C}_{sym}}(L-s) = \int_0^{L-s} \frac{d\vec{T}_{\mathcal{C}_{sym}}}{du} du - \vec{T}_f \\
&\overset{v=L-u}{=} \int_L^s \frac{d\vec{T}_{\mathcal{C}_{sym}}}{dv} dv - \vec{T}_f = -\int_s^L \frac{d\vec{T}_{\mathcal{C}_{sym}}}{dv} dv - \vec{T}_f \\
&= \int_s^L \frac{d\vec{T}_{\mathcal{C}}}{dv} dv - \vec{T}_f = \int_s^L \frac{d\vec{T}_{\mathcal{C}}}{dv} dv - \left(\int_0^L \frac{d\vec{T}_{\mathcal{C}}}{dv} dv + \vec{T}_0 \right) \\
&= -\int_0^s \frac{d\vec{T}_{\mathcal{C}}}{dv} dv - \vec{T}_0 = -\vec{T}_{\mathcal{C}}(s).
\end{aligned}$$

We now show that the curve $\mathcal{C}_{sym}$ coincides with the curve $\mathcal{C}$:

$$\begin{aligned}
&\mathcal{C}_{sym}(L-s) = \mathbf{x}_f + \int_0^{L-s} \left[\int_0^t \frac{d\vec{T}_{\mathcal{C}_{sym}}}{du} du - \vec{T}_f \right] dt \\
&\overset{v=L-u}{=} \mathbf{x}_f + \int_0^{L-s} \left[\int_L^{L-t} \frac{d\vec{T}_{\mathcal{C}_{sym}}}{dv} dv - \vec{T}_f \right] dt \\
&= \mathbf{x}_f + \int_0^{L-s} \left[\int_{L-t}^{L} \frac{d\vec{T}_{\mathcal{C}}}{dv} dv - \vec{T}_f \right] dt \\
&\overset{\hat{t}=L-t}{=} \mathbf{x}_f - \int_L^s \left[\int_{\hat{t}}^{L} \frac{d\vec{T}_{\mathcal{C}}}{dv} dv - \vec{T}_f \right] d\hat{t} \\
&= \mathbf{x}_f - \int_L^s \left[\int_{\hat{t}}^{L} \frac{d\vec{T}_{\mathcal{C}}}{dv} dv - \int_0^L \frac{d\vec{T}_{\mathcal{C}}}{dv} dv - \vec{T}_0 \right] d\hat{t} \\
&= \mathbf{x}_0 + \int_0^s \left[\int_0^{\hat{t}} \frac{d\vec{T}_{\mathcal{C}}}{dv} dv + \vec{T}_0 \right] d\hat{t} \overset{Eq.\ (2)}{=} \mathcal{C}(s). \;\; \square
\end{aligned}$$

B. EXTENSIBILITY (PROPOSITION 5.4)

Proof: Given a 3D Euler spiral $\mathcal{C}$ interpolating the point-tangent pairs $(\mathbf{x}_0, \vec{T}_0)$, $(\mathbf{x}_f, \vec{T}_f)$, we will show that for every $(\mathbf{x}_m, \vec{T}_m)$ on $\mathcal{C}$, the curves $\mathcal{C}_1$ between $\mathbf{x}_0$ and $\mathbf{x}_m$ and $\mathcal{C}_2$ between $\mathbf{x}_m$ and $\mathbf{x}_f$ coincide with $\mathcal{C}$, each in its own section.

Assume that $\mathcal{C}$ has parameters $\kappa_0, \tau_0, \gamma, \delta, L$. Let L_1 be the length of the sub-curve of $\mathcal{C}$ from $\mathbf{x}_0$ to $\mathbf{x}_m$. By the tangent definition and by Equation (2):

$$\vec{T}_m = \int_0^{L_1} \frac{d\vec{T}}{du} du + \vec{T}_0, \tag{11}$$

$$\mathbf{x}_m = \int_0^{L_1} \left[\int_0^t \frac{d\vec{T}}{du} du + \vec{T}_0 \right] dt + \mathbf{x}_0. \tag{12}$$

Below we first show that $\mathcal{C}_1$ with the parameters $\hat{\kappa_0} = \kappa_0, \hat{\tau_0} = \tau_0, \hat{\gamma} = \gamma, \hat{\delta} = \delta, \hat{L} = L_1$, coincides with $\mathcal{C}$ for $0 \leq s \leq L_1$. Then we show that $\mathcal{C}_2$ with the parameters $\widetilde{\kappa_0} = \kappa_0 + \gamma L_1, \widetilde{\tau_0} = \tau_0 + \delta L_1, \widetilde{\gamma} = \gamma, \widetilde{\delta} = \delta, \widetilde{L} = L - L_1$, coincides with $\mathcal{C}$ for $L_1 \leq s \leq L$. The latter is done in two steps: First we use Equation (11) to prove that the tangents are equal and then we use both Equations (11) and (12) to prove that the coordinates are the same.

The proof that $\mathcal{C}_1$ coincides with $\mathcal{C}$ for $0 \leq s \leq L_1$ is trivial and derived from Proposition 4.1. Since both curves have the same parameters, they must be the same curve, by the uniqueness of the curve.

Let us denote the tangent of the curve $\mathcal{C}$ at $\mathcal{C}(s)$ by $\vec{T}_{\mathcal{C}}(s)$ and the tangent of the curve $\mathcal{C}_2$ at $\mathcal{C}_2(s)$ by $\vec{T}_{\mathcal{C}_2}(s)$. In order to show that $\mathcal{C}_2$ coincides with $\mathcal{C}$, we need to show that a 3D Euler spiral $\mathcal{C}_2$ that starts at $(\mathbf{x}_m, \vec{T}_m)$ and has parameters $\widetilde{\kappa_0}, \widetilde{\tau_0}, \widetilde{\gamma}, \widetilde{\delta}, \widetilde{L}$, reaches $\mathcal{C}(s)$ with tangent $\vec{T}_{\mathcal{C}}(s)$, $\forall s$, $L_1 \leq s \leq L$.

We first show that $\forall s, L_1 \leq s \leq L$, the tangent at $\mathcal{C}_2(s - L_1)$ is $\vec{T}_{\mathcal{C}}(s)$. According to Definition 4.1, 2–4, we get:

$$\begin{aligned}
\frac{d\vec{T}_{\mathcal{C}_2}(u)}{du} &= (\kappa_0 + \gamma L_1 + \gamma u)\, \vec{N}_{\mathcal{C}_2}(u) \\
\frac{d\vec{N}_{\mathcal{C}_2}(u)}{du} &= -(\kappa_0 + \gamma L_1 + \gamma u)\, \vec{T}_{\mathcal{C}_2}(u) + (\tau_0 + \delta L_1 + \delta u)\, \vec{B}_{\mathcal{C}_2}(u) \\
\frac{d\vec{B}_{\mathcal{C}_2}(u)}{du} &= -(\tau_0 + \delta L_1 + \delta u)\, \vec{N}_{\mathcal{C}_2}(u),
\end{aligned}$$

and by the tangent definition:

$$\vec{T}_{\mathcal{C}_2}(s - L_1) = \int_0^{s-L_1} \frac{d\vec{T}_{\mathcal{C}_2}}{du} du + \vec{T}_m.$$

In a similar manner to the proof of Proposition 5.3, by defining a new integration parameter $v = u + L_1$ and substituting Equation (11), we get:

$$\begin{aligned}
&\vec{T}_{\mathcal{C}_2}(s - L_1) = \int_{L_1}^{s} \frac{d\vec{T}_{\mathcal{C}}}{dv} dv + \vec{T}_m \\
&= \int_{L_1}^{s} \frac{d\vec{T}_{\mathcal{C}}}{dv} dv + \int_0^{L_1} \frac{d\vec{T}_{\mathcal{C}}}{dv} dv + \vec{T}_0 = \int_0^{s} \frac{d\vec{T}_{\mathcal{C}}}{dv} dv + \vec{T}_0 = \vec{T}_{\mathcal{C}}(s).
\end{aligned}$$

Next, we show that $\forall s, L_1 \leq s \leq L$, $\mathcal{C}_2(s - L_1) = \mathcal{C}(s)$. By Equation (2), we can define the endpoint of $\mathcal{C}_2$ as follows:

$$\begin{aligned}
&\mathcal{C}_2(s - L_1) = \mathbf{x}_m + \int_0^{s-L_1} \left[\int_0^{t} \frac{d\vec{T}_{\mathcal{C}_2}}{du} du + \vec{T}_m \right] dt \\
&\overset{v=u+L_1}{=} \mathbf{x}_m + \int_0^{s-L_1} \left[\int_{L_1}^{t+L_1} \frac{d\vec{T}_{\mathcal{C}}}{dv} dv + \vec{T}_m \right] dt \qquad (13) \\
&\overset{\hat{t}=t+L_1}{=} \mathbf{x}_m + \int_{L_1}^{s} \left[\int_{L_1}^{\hat{t}} \frac{d\vec{T}_{\mathcal{C}}}{dv} dv + \vec{T}_m \right] d\hat{t}.
\end{aligned}$$

Substituting Equation (12) into Equation (13) and then substituting Equation (11) will give us:

$$\begin{aligned}
&\mathcal{C}_2(s - L_1) = \\
&= \mathbf{x}_0 + \int_0^{L_1} \left[\int_0^{\hat{t}} \frac{d\vec{T}_{\mathcal{C}}}{dv} dv + \vec{T}_0 \right] d\hat{t} + \int_{L_1}^{s} \left[\int_{L_1}^{\hat{t}} \frac{d\vec{T}_{\mathcal{C}}}{dv} dv + \vec{T}_m \right] d\hat{t} \\
&= \mathbf{x}_0 + \int_0^{L_1} \left[\int_0^{\hat{t}} \frac{d\vec{T}_{\mathcal{C}}}{dv} dv + \vec{T}_0 \right] d\hat{t} + \int_{L_1}^{s} \left[\int_0^{\hat{t}} \frac{d\vec{T}_{\mathcal{C}}}{dv} dv + \vec{T}_0 \right] d\hat{t} \\
&= \mathbf{x}_0 + \int_0^{s} \left[\int_0^{\hat{t}} \frac{d\vec{T}_{\mathcal{C}}}{dv} dv + \vec{T}_0 \right] d\hat{t} = \mathcal{C}(s),
\end{aligned}$$

where the last equality holds by Equation (2). □